Distributed Vibration Sensing Over 125 km With Enhanced SNR Using Phi-OTDR Over a URFL Cavity

Hugo F. Martins, Sonia Martin-Lopez, Pedro Corredera, Juan Diego Ania-Castañon, Orlando Frazão, and Miguel Gonzalez-Herraez, *Senior Member, OSA*

***Abstract*—We describe the use of a phase-sensitive optical time domain reflectometer (ϕOTDR) over an ultra-long Raman fiber laser cavity allowing fully distributed detection of vibrations over 125 km. Compared to a first-order Raman-assisted ϕOTDR, this scheme shows an enhanced signal-to-noise ratio (SNR). This is due to the fact that the relative intensity noise introduced by the Raman amplification is mostly transferred to a lower frequency range, where the balanced detection implemented in the setup provides better suppression of the common-mode noise. The sensor was able to measure vibrations of up to 380 Hz (limit set by the time of flight of light pulses) in a distance of 125 km with a resolution of 10 m and an average SNR of 8 dB with no postprocessing. This implies a >3 dB improvement in SNR over a first-order Raman-assisted setup with similar characteristics.**

***Index Terms*—Distributed sensor, optical fiber sensors, phase-sensitive OTDR, Raman scattering, vibration sensor.**

I. Introduction

FOR more than twenty years phase-sensitive optical time domain reflectometry (ϕOTDR) has been widely studied and reported in the scientific literature [1]–[12] due to its potential for fully distributed monitoring of vibrations along an optical fiber cable. This capability turns out to be very attractive for intrusion monitoring over large perimeters [1].

Traditional ϕOTDR sensors have been demonstrated to allow the measurement of distributed vibrations of up to 40 kHz [2]. Dynamic ranges of a few tens of kilometers with spatial resolutions in the range of meters have also been reported [3] using these systems. The reliability of ϕOTDR systems has also been proven in field tests by successfully detecting people walking on top of a buried fiber [4]. ϕOTDR systems can also be used for temperature and strain measurements by analyzing the cross-correlation of ϕOTDR traces with different input wavelength pulses [5].

In ϕOTDR operation, dynamic range, resolution, and signal-to-noise ratio (SNR) are closely related parameters. Although for a given resolution the increase of the ϕOTDR input pump peak power will increase the dynamic range and SNR, this approach is limited due to the onset of nonlinear effects [6]. Although specific signal post-processing can improve the performance of a ϕOTDR [7], a significant increase of the sensing range can only be achieved using optical amplification [8]–[12]. In particular, distributed Raman amplification seems an ideal route to achieve this range enhancement, as the amplification can be engineered to keep the power of the optical pulse almost constant along the whole fiber length.

A number of different architectures using Raman amplification have been proposed to assist distributed [10]–[15] and point [16] fiber sensors. Different pumping configurations have been studied using first [10]–[14], second [11], [15], and even third-order [17] Raman amplification. The noise introduced by the Raman gain process, mainly due to relative intensity noise (RIN) transfer from the Raman pumps, is one of the main concerns when using this type of amplification [18], [19]. If not carefully handled, this can completely mask the signal. In ϕOTDR operation, Raman amplification can be combined with balanced detection to reduce the RIN transfer from the Raman pumps. With this combination, it has been demonstrated the possibility to extend the sensing range beyond 100 km [10], [11]. Recently, Brillouin amplification has also been proposed to increase the sensing range of ϕOTDR for vibration sensing. In this case, however, the gain is temperature dependent which can lead to instability of the system [8], [9].

In this letter, we demonstrate a significant range extension in a ϕOTDR sensor by creating an ultra-long Raman fiber laser cavity (URFL) in the sensing fiber. The key advantage of this setup over a first-order Raman assistance setup [10], [11] is that the RIN is transferred mostly in a frequency band below 5 MHz (unlike the first-order setup which entails significant RIN noise up to 100 MHz). By implementing a suitable balanced detection, the RIN noise is completely eliminated. The sensor was able to measure vibrations of up to 380 Hz (limit set by the time of flight of light pulses) in a distance of 125 km with a resolution of

Manuscript received September 13, 2014; revised November 19, 2014; accepted December 29, 2014. Date of publication January 25, 2015; date of current version April 29, 2015. This work was supported in part by funding from the European Research Council under Starting Grant U-FINE (Grant 307441), EU-FP7 ITN ICONE, the Spanish "Plan Nacional de I+D+i" under Projects TEC2012-37958-C02-01, TEC2012-37958-C02-02, TEC2011-27314, TEC2013-45265-R, the regional Program SINFOTON-CM: S2013/MIT-2790 funded by the Comunidad de Madrid and the INTERREG SUDOE Program ECOAL-MGT. The work of S. Martin-Lopez was supported by the Spanish Ministry of Science and Innovation under a "Ramón y Cajal" Contract.

H. F. Martins is with the FOCUS S.L., 28004 Madrid, Spain (e-mail: hugo.martins@focustech.eu).

S. Martin-Lopez and M. Gonzalez-Herraez are with the Departamento de Electrónica, Universidad de Alcalá, 28871 Madrid, Spain (e-mail: sonia.martin@depeca.uah.es; miguelg@depeca.uah.es).

P. Corredera and J. D. Ania-Castañon are with the Instituto de Óptica, CSIC, 28006 Madrid, Spain (e-mail: p.corredera@csic.es; jd.ania@csic.es).

O. Frazão is with the Faculdade de Ciências da Universidade do Porto, 4169 007 Porto, Portugal, and also with the INESCTEC, 4169-007 Porto, Portugal (e-mail: ofrazao@fc.up.pt).

Color versions of one or more of the figures in this paper are available online at http://ieeexplore.ieee.org.

Digital Object Identifier 10.1109/JLT.2015.2396359

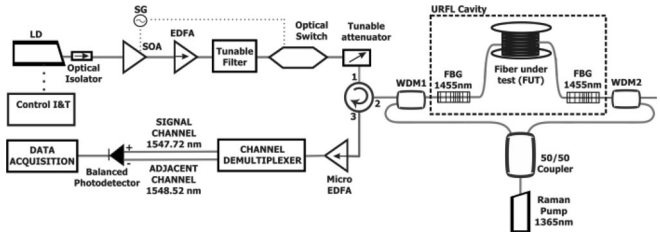

Fig. 1. Experimental Setup: Acronyms are explained in the text.

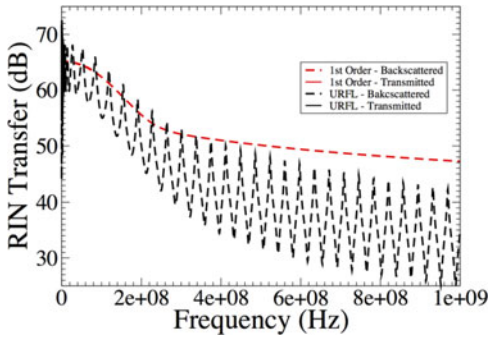

Fig. 2. RIN transfer functions from URFL (black) and first-order (red) pumps to the transmitted (solid) and backscattered (dashed) signals in a 125 km span. First-order pump power is 27.4 dBm per pump (full attenuation compensation). URFL pump power is 28.5 dBm per pump. Signal peak power: 10 mW.

10 m. Since no post-processing, extremely high coherence lasers or coherent detection methods are required, the complexity of the scheme is also kept to a minimum. A clear improvement of the performance of the sensor when compared to vibration measurements using first-order Raman amplification [10], [11] under similar conditions is demonstrated. Also, the ϕOTDR trace presented higher flatness and therefore higher amplitude of oscillations in the lower sensitivity points. The sensor was able to measure vibrations until a higher frequency and with higher SNR in these points.

II. Experimental Setup and Theoretical Background

The experimental setup used to characterize the ϕOTDR over an URFL cavity (shown in Fig. 1) is based on a couple of minor adaptations of the setup used by the same authors to characterize first-order Raman amplification [10]:(1) a second-order URFL scheme was used in the sensing fiber (instead of first-order Raman) and (2) a different tunable filter was used.

A laser diode driven by a standard current and temperature controller with a linewidth of 1.6 MHz emitting at 1548 nm was used as the master source, followed by an optical isolator (ISO). A semiconductor optical amplifier (SOA), with rise/fall times in the order of 2.5 ns, driven by a waveform signal generator was used to create 100 ns almost square pulses. Between the signal pulses, the SOA was negatively biased so as to enhance the ER of the delivered pulses. An ER of $>$50 dB was achieved this way. An Erbium-Doped Fiber Amplifier (EDFA) was used to boost the power of the ϕOTDR input pulses and reach peak powers in the pulse of several hundred milliwatts. It was followed by a tunable filter which presented an approximate gaussian profile with 0.2 nm full width at half maximum (FWHM) and was used to minimize the effect of the ASE added by the EDFA. As previously demonstrated [2], the ER greatly affects the performance of a ϕOTDR in normal operation. Although the use of a SOA allows achieving a high extinction ratio (ER) ($>$50 dB), an optical switch may be useful to "window" the input pulses and further increase their ER, especially when the distance to be monitored is very large [10]. In this case, an optical switch with rise/fall times of 200 ns and a typical ER of 25 dB was used after the tunable filter in order to further increase the ER of the pulses and reduce the noise delivered into the fiber outside the pulse. It was driven so as to have a sub-microsecond transmission window synchronized with the pulse. After that, light passed through an attenuator, which allowed varying the input pulse power in the fiber.

The fiber under test (FUT), is connected to the common ports of two WDMs (1310/1550 nm). The input pulse is launched into the FUT through the 1550 nm (1460–1620 nm) port of the WDM1. The primary Raman pump is a Raman Fiber Laser (RFL) emitting at 1365 nm with a RIN <-105 dBc/Hz. The power of this laser can be tuned up to 5 W. The RFL beam is divided by a calibrated 50/50 coupler in two beams and each beam is then coupled into the 1310 nm (1270–1350 nm) ports of the WDMs. Two FBGs centered at 1455 nm with 0.5 nm FWHM and with 80% reflectivity are placed in both ends of the fiber, thus creating the URFL cavity. It is important to understand the dynamics of this URFL in order to understand the advantage of this setup over first-order Raman assist. The URFL has itself a resolvable mode structure, with a spectral mode spacing of $\Delta\upsilon \approx 0.8\,\mathrm{kHz} = c/(2nL)$, where c is the velocity of the light in the vacuum, n the refractive index and L the FUT length. In practice however, and depending on the pump power applied, the mode structure can be partially or totally erased due to Rayleigh backscattering and the four-wave mixing between the multiple modes [20].

URFL amplification is a particular case of second-order, bidirectional Raman amplification. The RIN transfer function in bidirectionally-pumped distributed amplification systems displays a characteristic staircase structure with two superimposed cut-off frequencies due to the different relative speeds of the amplified signal to the co- and counter-propagating pumps. This effect is less noticeable for the Rayleigh backreflected signals received in an OTDR, since they reach the receiver after having propagated both co- and counter-directionally to both pumps. Frequencies for the cut-off points appear at a lower value in the case of second-order URFL amplification than they do in non-laser amplified schemes [19]. In addition, URFLs present a much steeper slope in the filtering of high frequencies. Hence, URFL-assisted ϕOTDR can be expected to present less RIN noise at high frequencies (above the 10's of MHz) than typical first-order Raman amplified ones [10], [11].

Fig. 2 illustrates this issue by comparing the calculated RIN transfer functions from the Raman pumps to the transmitted and Rayleigh backreflected signal, for the cases of URFL and first-order Raman amplification. These traces have been obtained through numerical simulation, following the model presented in [19].

This reduction of noise at high frequencies is a key advantage of the URFL system, as the balanced detection implemented in

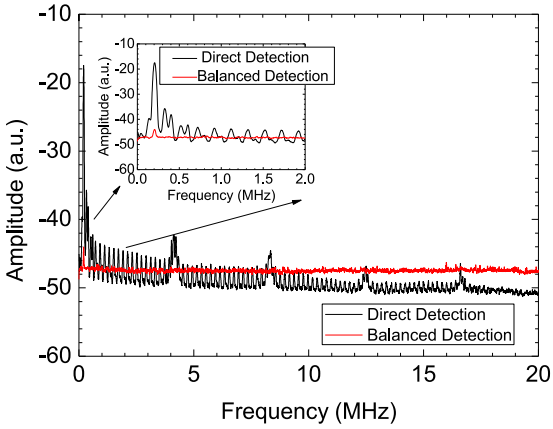

Fig. 3. Characterization of the noise in the electrical spectrum domain of the signal returning from the fiber when a Raman pump power of 28.5 dBm is launched on both ends of the FUT without input ϕOTDR pump using balanced and direct detection. While balanced detection only presents white noise and a small peak at 0.2 MHz, the direct detection presents higher noise levels and periodical structure with peaks every 0.2 MHz.

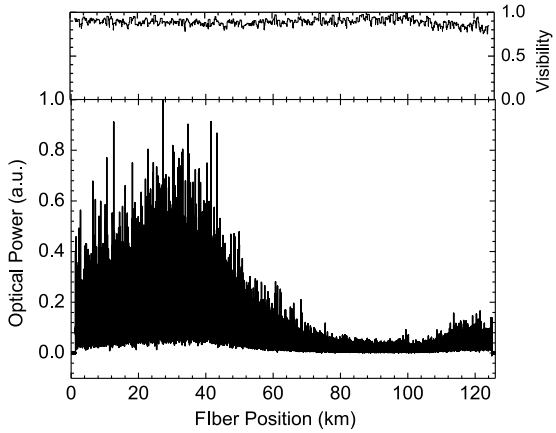

Fig. 4. ϕOTDR interference signal along the FUT when the Raman pump power launched on each end of the FUT was 28.5 dBm. In this case, the ϕOTDR pump power was chosen as the one ensuring the best performance. The top figure shows the visibility of the interference signal, computed as $V = (T_{\max} - T_{\min})/(T_{\max} + T_{\min})$ where $T_{\max}$ and $T_{\min}$ are the maximum and minimum values of the trace over a window of 500 m.

the setup will provide a better suppression of the common-mode noise. The power variation of the URFL along the FUT will also be lower than the power variations of the primary RFL pumps.

The signal back-reflected from the fiber is amplified (using a micro-EDFA) and then goes through a 100 GHz channel demultiplexer which filters out the channel of the signal (centered at 1547.72 nm) and an adjacent channel (centered at 1548.52 nm), thus filtering out the ASE added by the micro-EDFA. These channels are then coupled to the "+" and "−" port of a p-i-n balanced photodetector with amplification and 100 MHz bandwidth. Since the optical paths leading to the "+" and "−" ports are the same (within 1 cm tolerance), an effective cancelation of the RIN noise is ensured. The signal was then recorded using a high-speed digitizer.

Fig. 3 shows the signal returning from the fiber in the electrical spectrum domain when a 28.5 dBm Raman pump power was launched on each side of the FUT without input ϕOTDR pump for direct and balanced detection. This was observed as the best Raman pump power for balanced detection (and was later used for the measurements) since for higher powers the noise of the signal was observed to increase abruptly, due to strong RIN transfer from the Raman pumps. As we see, most of the RIN noise in this case is transferred in a frequency region below 5 MHz, where the balanced detection should be very effective eliminating the noise. In this case, the overall RIN noise should be lower than when using a first-order Raman amplified setup assisted by balanced detection [10], [11], without significantly increasing the low frequency RIN noise.

As expected, the direct detection performed much worse [10]. A periodical structure was observed, with peaks every 0.2 MHz, correspondent to the cavity length of the RFL (∼500 m). In addition, peaks with ∼4 MHz spacing appeared in the electrical spectrum, corresponding to the cavity round-trip time of the Yb master pump laser in the RFL.

In the balanced detection case, only white noise and a small peak at 0.2 MHz (which presented a reduction of ∼30 dB when compared to the direct case) were observed, for the same Raman pump powers. This strong reduction of low frequency noise is key to the presented setup, as low frequency components are the most harmful when dealing with vibration detection. This is due to the fact that low frequency noise introduces noise peaks in the time-domain signals for given points of the fibre, which can overlap the vibration signals.

Since balanced detection uses the difference between two channels, it is expected to present a 3 dB higher noise than direct detection at high frequencies where the RIN noise is no longer as much of an issue, or balanced detection is not as efficient. However, the demonstrated advantages of the strong reduction of the low frequency RIN noise peaks, far surpass this drawback in the presented setup.

Fig. 4 shows the ϕOTDR trace recorded with a Raman pump power launched on each end of the FUT of 28.5 dBm. The input ϕOTDR pump peak power was estimated to be below 10 mW and was chosen as the highest possible power before the appearance of nonlinearities (mainly MI, which leads to a fast decrease of the visibility) [6]. This way, the best performance along all points of the fiber is ensured. As expected, random oscillations are observed along the trace. The FUT was the same which was used to test first-order Raman amplification over 125 km [10], [11] and it consisted of two fiber spools of 50 km and one fiber spool of 25 km of SMF-28, all linked by optical connectors. Due to a connector loss at ≈98 km (estimated in 3 dB) a decrease of the amplitude of the trace oscillations is observed in that point. The vibrations were measured immediately after this connector loss, as it was clearly the worst sensitivity point along the fiber. Although better results could be obtained if the fiber was spliced in this point (the amplitude drop of the trace oscillations would not occur), this loss was kept in order to provide a reliable comparison of the results using first-order Raman amplification and the URFL, and also to demonstrate that the system can detect vibrations over 125 km even under non-ideal conditions, as the vibrations were clearly measured. Another advantage of using the URFL over first-order Raman amplification is clear as

the trace presents higher flatness along the fiber under similar measurement conditions [10], [11]. This ensures the best performance as higher amplitude of oscillations and therefore higher SNR is achieved in the lowest sensitivity point. The visibility of the ϕOTDR trace along the FUT, calculated as indicated in the figure caption, is presented in the top figure. Although the amplitude of the oscillations of the ϕOTDR trace varies along the FUT, the visibility remains close to 1 (even after the connector loss), i.e., the interference does not lose contrast along the propagation. In this case, the sensor is shown to perform reliable vibration measurements at any position along the FUT if reliable vibration measurements are demonstrated in the position of worst signal level (after the connector loss, around km 98). For this reason, the vibration measurement tests are done in this position.

III. Vibration Measurements

The procedure used to perform the vibration measurements was similar to the one used in [10], [11], in order to provide a reliable comparison of the results using the URFL and first-order Raman amplification. The power evolution as a function of time for each point along the FUT was obtained by monitoring equivalent points in consecutive traces. The FFT of this power evolution will therefore present the frequencies measured for each point.

The sampling frequency of our sensor will be the input ϕOTDR pump pulse repetition rate, which in this case was 781 Hz. Theoretically, this limits the maximum fiber span to be monitored to 131 km and the maximum detectable frequency to 390 Hz (Nyquist theorem). As for the Raman and input ϕOTDR pump powers they were the same as the ones used in Fig. 4.

As demonstrated in Fig. 4, the position of worst signal level of the trace (lowest amplitude oscillations of the trace) was after the connector at km 98. Vibrations were applied to this point by placing the fiber inside a 2 m long PVC tube with 0.08 m of diameter in which mechanical vibrations of controllable frequency were applied using a small vibration exciter with a maximum bare table acceleration of 736 ms^{-2} (with a 75 g mass attached). In order to avoid the propagation of vibrations outside the PVC tube, the fiber was clamped at its exits. Frequencies between 20 Hz and 380 Hz (nearly the theoretical maximum detectable by the sensor) were applied to the PVC tube and the FFT spectra of the optical power variation recorded by the ϕOTDR at this position is presented in Fig. 5. In this case, for the range of frequencies applied, the estimated displacement of the PVC tube is estimated to be in the sub-millimeter range. The sensor was able to successfully detect all the vibration frequencies applied, presenting peaks with amplitude 6–10 times higher than the noise level in the rest of the spectrum of the FFT, i.e., a SNR of 8–10 dB. The presented sensor was therefore able to detected vibrations until higher frequencies and with a SNR improvement of ≈4–5 dB when compared to the case where first-order Raman amplification was used [10], [11], where vibrations of up to 250 Hz with a SNR of 3–6 dB were detected under similar measurement conditions.

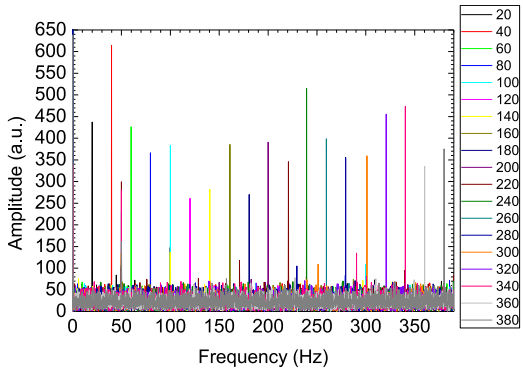

Fig. 5. FFT spectra of the optical power variation of the ϕOTDR signal for consecutive traces in the point of the FUT with minimum signal for applied frequencies between 20 Hz and 380 Hz, using the same conditions of Fig. 4.

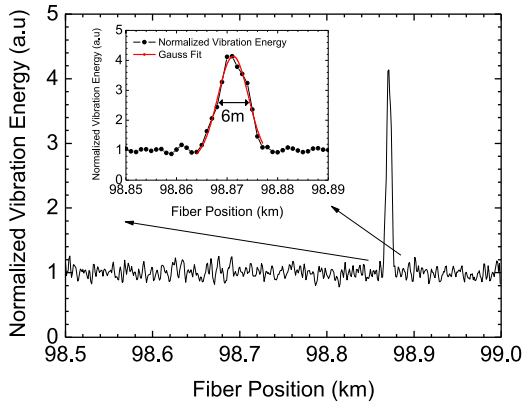

Fig. 6. Normalized energy density of vibrations around 20 Hz along the FUT when a vibration of 20 Hz was applied to the PVC tube (at ∼98.8 km). The normalized vibration energy density of the frequencies around 20 Hz was calculated for each fiber position as the RMS of the interval 18–22 Hz (signal) divided by the RMS of the interval 350 Hz-390 Hz (noise) of the FFT of the optical power variation of the ϕOTDR signal. In the inset figure a gaussian fit of the points where the vibration was detected is shown, presenting 6 m at FWHM.

The frequency of 50 Hz was also recorded in the vibration measurements due to the proximity of electrical instruments. It is important to notice that the presented data does not include any post-processing and therefore there is room for improvement of the performance of the sensor if adequate signal processing is used for specific applications.

Fig. 6 shows the normalized energy of vibrations around 20 Hz, (calculated as indicated in the figure caption) along the FUT when a vibration of 20 Hz was applied to the PVC tube (located at ≈98.8 km). In the points which are not affected by the vibration, the energy of the vibrations around 20 Hz is comparable to the energy of the noise and the normalized vibration energy is ≈1. In the points affected by the vibration however, the energy of the vibrations around 20 Hz is higher than the noise. In this case, the energy of the vibrations increased by more than 4 times in the points of the fiber where vibration was applied. The vibration was applied along 2 m of fiber and an increase of energy vibration was detected along 11 m of fiber (98865–98876 m). This means that the resolution without any

further processing is $\sim$10 m, as it was expected considering an input ϕOTDR pump pulse width of 100 ns.

IV. Conclusion

To the best of our knowledge, a description of the use of a ϕOTDR over an URFL cavity for the distributed detection of vibrations is presented for the first time. The sensor was able to measure vibrations of up to 380 Hz (limit set by the time of flight of light pulses) in a distance of 125 km with a resolution of 10 meters. A clear improvement of the performance of the sensor both in vibration measuring range and SNR when compared to vibration measurements using first-order Raman amplification under similar conditions is demonstrated. The monitoring of intrusions over large structures such as national borders, military bases or pipelines are a few of the possible applications for this sensor.

References

[1] H. F. Taylor and C. E. Lee, "Apparatus and method for fiber optic intrusion sensing," U.S. Patent 5 194 847, Mar. 16, 1993.

[2] H. F. Martins, S. Martin-Lopez, P. Corredera, M. L. Filograno, O. Frazao, and M. Gonzalez-Herraez, "Coherent noise reduction in high visibility phase sensitive optical time domain reflectometer for distributed sensing of ultrasonic waves," *J. Lightw. Technol.*, vol. 31, no. 23, pp. 3631–3637, Dec. 2013.

[3] J. C. Juarez and H. F. Taylor, "Field test of a distributed fiber-optic intrusion sensor system for long perimeters," *Appl. Opt.*, vol. 46, no. 11, pp. 1968–1971, 2007.

[4] J. C. Juarez, E. W. Maier, K. N. Choi, and H. F. Taylor, "Distributed fiber-optic intrusion sensor system," *J. Lightw. Technol.*, vol. 23, no. 6, pp. 2081–2087, Jun. 2005.

[5] Y. Koyamada, M. Imahama, K. Kubota, and K. Hogari, "Fiber-optic distributed strain and temperature sensing with very high measurand resolution over long range using coherent OTDR," *J. Lightw. Technol.*, vol. 27, no. 9, pp. 1142–1146, May 2009.

[6] H. F. Martins, S. Martin-Lopez, P. Corredera, P. Salgado, O. Frazão, and M. Gonzalez-Herraez, "Modulation instability-induced fading in phase-sensitive optical time-domain reflectometry," *Opt. Lett.*, vol. 38, no. 6, pp. 872–874, 2013.

[7] Z. Qin, L. Chen, and X. Bao, "Wavelet denoising method for improving detection performance of distributed vibration sensor," *IEEE Photon. Technol. Lett.*, vol. 24, no. 7, pp. 542–544, Apr. 2012.

[8] Z. Wang, J. Li, M. Fan, L. Zhang, F. Peng, H. Wu, J. Zeng, Y. Zhou, and Y. Rao, "Phase-sensitive optical time-domain reflectometry with Brillouin amplification," *Opt. Lett.*, vol. 39, no. 15, pp. 4313–4316, 2014.

[9] Z. Wang, J. Zeng, J. Li, M. Fan, H. Wu, F. Peng, L. Zhang, Y. Zhou, and Y. Rao, "Ultra-long phase-sensitive OTDR with hybrid distributed amplification," *Opt. Lett.*, vol. 39, no. 20, pp. 5866–5869, 2014.

[10] H. F. Martins, S. M. Lopez, P. Corredera, M. L. Filograno, O. Frazão, and M. G. Herráez, "Phase-sensitive optical time domain reflectometer assisted by first-order Raman amplification for distributed vibration sensing over $>$100 km," *J. Lightw. Technol.*, vol. 32, no. 8, pp. 1510–1518, Apr. 2014.

[11] H. F. Martins, S. Martin-Lopez, M. L. Filograno, P. Corredera, O. Frazão, and M. Gonzalez-Herraez, "Comparison of the use of first and second-order Raman amplification to assist a phase-sensitive optical time domain reflectometer in distributed vibration sensing over 125 km," *Proc. SPIE*, vol. 9157, pp. 91576K-1–91576K-4, Jun. 2014.

[12] F. Peng, H. Wu, X. Jia, Y. Rao, Z. Wang, and Z. Peng, "Ultra-long high-sensitivity -OTDR for high spatial resolution intrusion detection of pipelines," *Opt. Exp.*, vol. 22, no. 11, pp. 13804–13810, 2014.

[13] M. Alahbabi, Y. Cho, and T. Newson, "150-km-range distributed temperature sensor based on coherent detection of spontaneous Brillouin backscatter and in-line Raman amplification," *J. Opt. Soc. Am. B*, vol. 22, no. 6, pp. 1321–1324, 2005.

[14] F. Rodriguez-Barrios, S. Martin-Lopez, A. Carrasco-Sanz, P. Corredera, J. D. Ania-Castanon, L. Thevenaz, and M. Gonzalez-Herraez, "Distributed Brillouin fiber sensor assisted by first-order Raman amplification," *J. Lightw. Technol.*, vol. 28, no. 15, pp. 2162–2172, Aug. 2010.

[15] S. Martin-Lopez, M. Alcon-Camas, F. Rodriguez-Barrios, P. Corredera, J. D. Ania-Castanon, L. Thevenaz, and M. Gonzalez-Herraez, "Brillouin optical time-domain analysis assisted by second-order Raman amplification," *Opt. Exp.*, vol. 18, no. 18, pp. 18769–18778, 2010.

[16] H. F. Martins, M. B. Marques, and O. Frazao, "300 km-ultralong Raman fiber lasers using a distributed mirror for sensing applications," *Opt. Exp.*, vol. 19, no. 19, pp. 18149–18154, 2011.

[17] X. Jia, Y. Rao, Z. Wang, W. Zhang, Z. Ran, K. Deng, and Z. Yang, "Detailed theoretical investigation on improved quasi-lossless transmission using third-order Raman amplification based on ultralong fiber lasers," *J. Opt. Soc. Am. B*, vol. 29, no. 4, pp. 847–854, 2012.

[18] B. Bristiel, S. Jiang, P. Gallion, and E. Pincemin, "New model of noise figure and RIN transfer in fiber Raman amplifiers," *IEEE Photon. Technol. Lett.*, vol. 18, no. 8, pp. 980–982, Apr. 2006.

[19] M. Alcón-Camas and J. Ania-Castañón, "RIN transfer in 2nd-order distributed amplification with ultralong fiber lasers," *Opt. Exp.*, vol. 18, no. 23, pp. 23569–23575, 2010.

[20] S. K. Turitsyn, J. D. Ania-Castañón, S. A. Babin, V. Karalekas, P. Harper, D. Churkin, S. I. Kablukov, A. E. El-Taher, E. V. Podivilov, and V. K. Mezentsev, "270-km ultralong Raman fiber laser," *Phys. Rev. Lett.*, vol. 103, no. 13, pp. 133901-1–133901-4, 2009.

Authors' biographies not available at the time of publication.